Observations of Various Steady State and Dynamic Thermal Behaviors in a Continuous Casting Mold

Ronald J. O'Malley
Armco Technology Center
705 Curtis Street
Middletown, OH 45044
(513) 727-5708

Key Words: mold temperature, mold thermal analysis, mold heat transfer, stainless steel, carbon steel, thin slab casting, continuous casting

INTRODUCTION

Specific examples of some of the more interesting steady state and transient thermal behaviors that have been observed with the straight, parallel, thin slab continuous casting mold at Armco's Mansfield Operations are presented. Through the use of mold instrumentation, steady state thermal profiles that were obtained while casting low carbon steels, 409 stainless steels, and 430 stainless steels are compared and contrasted under similar casting conditions. The effects of several types of process upsets, such as SEN failures and mold level upsets, on the resultant transient thermal profiles in the mold are examined. Observations of thermal transients with time scales that range from seconds to hours in duration are also presented and discussed, using tools that allow the mold temperature profile to be viewed in animation.

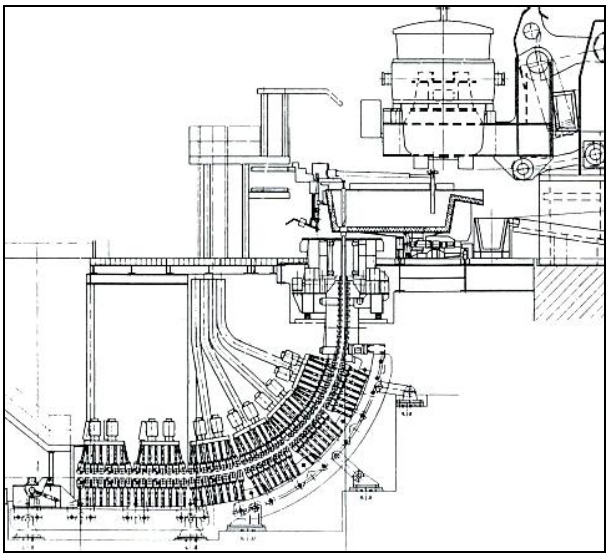

Figure 1 - Armco's medium-thin slab caster at Mansfield Operations.

EXPERIMENTAL

The new medium-thin slab caster at Armco's Mansfield Operations, shown in **Figure 1**, employs a 1.2 meter long straight parallel mold to cast carbon steels and ferritic stainless steels by a direct charge routing without slab conditioning. To support the development of casting practices for direct hot charge stainless production, and to develop an improved understanding of the thermal behavior of Mansfield's unique plane-parallel thin slab mold, an instrumented mold was constructed as part of a joint project with Voest Alpine Industrieanlagenbau GmbH[1]. This mold was operated on a campaign basis to assist in the development of casting practices at Mansfield.

Mold Instrumentation

The instrumented mold that was employed for casting practice development at Mansfield consists of a dedicated mold cassette assembly that is equipped with 106 thermocouples that meas-

ure the mold plate temperature at various positions within mold. Thermocouple junctions were formed by welding a Constantan alloy stud to the bottom of a small flat bottom hole that was bored into the copper mold plate from the cassette side, thereby using the copper mold plate to form one leg of a type T thermocouple junction. The studs were sealed by a compression seal to isolate the thermocouple junction from the mold cooling water[2]. The wire leads to each junction were contained entirely within the cassette assembly. All connections were made using type T compensating wire and water tight connectors with type T compensating connecting pins. The location of the thermocouples on each symmetrical pair of mold cassettes is shown in **Figure 2**.

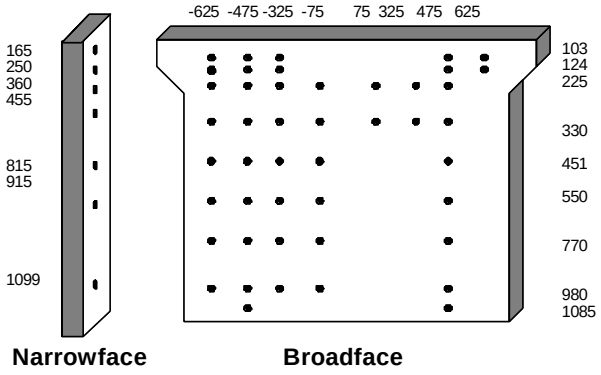

Figure 2 - Location of thermocouples in the instrumented mold (in mm).

Mold temperatures were collected using a dedicated computer and data logger that also recorded casting speed and mold level at rates of up to 1 Hz. Under normal conditions, data was collected at 5 second intervals. Supplemental process data was also collected from the caster level 2 system at 5 second intervals. This supplemental data consisted of process variables such as tundish weight, stopper rod position, mold water flows, mold water temperatures, secondary cooling flows, etc. An example of some typical mold temperature data collected by this procedure is shown in **Figure 3**.

Data Analysis

The mold thermocouple data was evaluated in a number of ways to examine the steady state and transient thermal behavior of the mold. Simple plots of temperature vs. time were prepared for selected arrays of thermocouples located at common width locations to compare temperatures at different distances from mold level. "Steady state" thermal analysis was conduced by evaluating average mold plate temperatures during a short period of steady state operation as a function of position in the mold. The standard deviation of these "steady state" temperatures was also evaluated. In some cases, the mold temperatures were also examined in the frequency domain using FFT analysis.

Mold thermal modeling was also employed to extract more meaningful information from the mold temperature data, such as mold hot face temperature, cold face temperature, hot face heat flux, etc. Special data visualization tools were also constructed to allow the temperature profiles in the mold to be examined during each 1-5 second data collection cycle, both discretely and in animation.

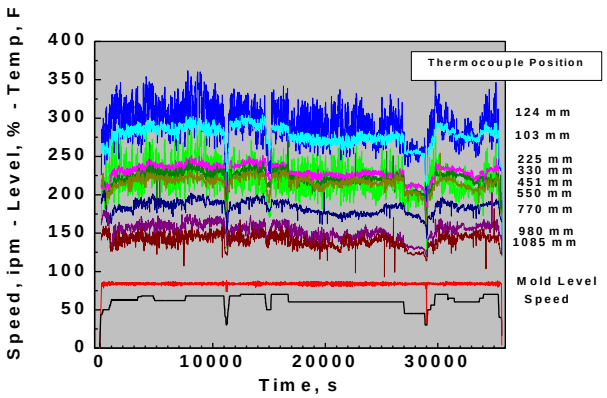

Figure 3 - Typical temperature data from an 8 heat sequence of 409 from the loose broadface thermocouple array 475 mm east of mold center.

RESULTS

The instrumented mold has been employed at Mansfield to collect and examine mold thermal data for some 94 heats since its introduction in late 1995. To date, mold thermal data has been collected for 1006 and 4130 carbon steels and for 409, 430, 434, 410, 435, and 436 stainless steels. Many of these grades were examined for a number of different casting conditions while casting practices were being developed and refined at Mansfield. Examples for three steel grades, a 1006 carbon steel, a 409 stainless steel, and a 430 stainless steel are presented here, using several different methods of analysis.

Steady State Analysis

The most common form of analysis of time based thermal data is to evaluate average temperatures as a function of position in the mold under "constant" casting conditions, i.e., constant speed, width, SEN submergence, casting temperature, etc. Plots like the one shown in **Figure 4** have been used widely by many investigators[3,4,5,6,7,8] to assess the temperature uniformity across the width of the mold and the shape of the temperature profile along the length of the mold under differing "steady state" casting conditions.

Often, standard deviations or maximum and minimum temperatures are included on these "steady state" plots[6] to provide an indication of the variability in temperature as a function of the position in the mold. Profiles of the standard deviations in the mold temperatures, like the one shown in **Figure 5,** have also been used[5] to identify the areas within the mold that have the greatest amount of variability in heat removal, thereby helping to develop strategies for improving mold lubrication.

The temperature measurements and their standard deviations shown in **Figures 4 and 5** for a 409 stainless steel show that the mold temperatures are relatively uniform across the broadface and that the temperature profile along the length of the mold varies as expected on the Mansfield mold, with peak temperatures occurring somewhat below the steel level (which is 104 mm from the top of the mold). The variability in temperature is also as expected, with the exception that the standard deviations in temperature are high on the narrowface midway down the length of the mold.

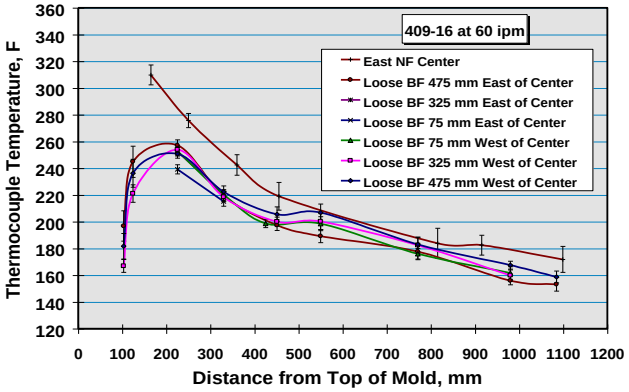

Figure 4 - Steady state mold temperatures and standard deviation in measured temperatures for 409 stainless cast at 60 ipm.

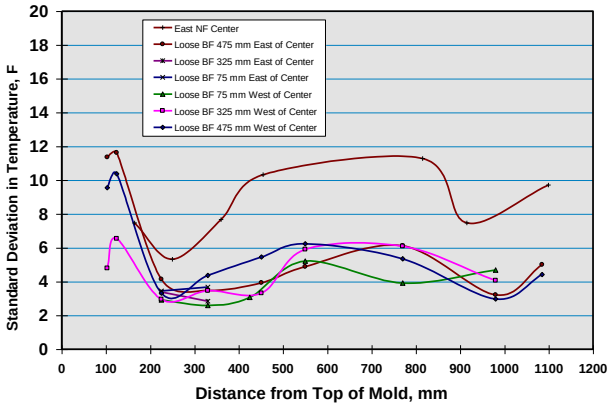

Figure 5 - Standard deviation in measured temperatures for 409 stainless cast at 60 ipm.

While the mold plate thermocouple temperatures can provide meaningful information about the conditions within the mold during casting, more meaningful data on the thermal condition of the mold can only be obtained by combining temperature measurements with a mold thermal model to extract information such as hot and cold face temperatures and heat fluxes. To accomplish this, a two dimensional thermal model[9] of Mansfield's 1.2 meter long straight parallel mold has been employed to calculate the hot face heat flux profile and other thermal conditions in the mold using the measured mold plate temperatures and the measured mold cooling water temperature rise as inputs to the mold thermal model.

A comparison of the predicted heat flux profiles and the predicted and measured thermocouple temperatures obtained using the model is shown in **Figures 6** through **8** for 1006 carbon steel, 409 stainless, and 430 stainless, respectively, at comparable casting speeds. In all cases, the heat flux curves were fitted to provide agreement with the measured temperature profile and the independently measured mold water temperature rise.

Another approach that has been employed to analyze mold temperature variations under steady state conditions is to examine the mold thermal data in the frequency domain using FFT analysis[10]. An example of this is shown in **Figure 9**, which shows a section of steady state mold level and temperature data at different positions along the length of the mold in the time domain and in the frequency domain. These analyses have been useful in determining how disturbances in mold level are propagated along the length of the mold, and what the key frequencies of these disturbances are. Interestingly, these analyses have tended to show that, even with relatively large fluctuations in mold level, the mold level disturbances do not propagate very far below the

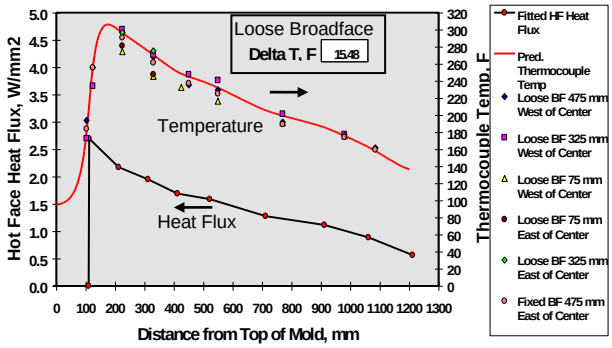

Figure 6 - Steady state temperature profile and calculated loose broadface heat flux for 1006 carbon steel at 59 ipm.

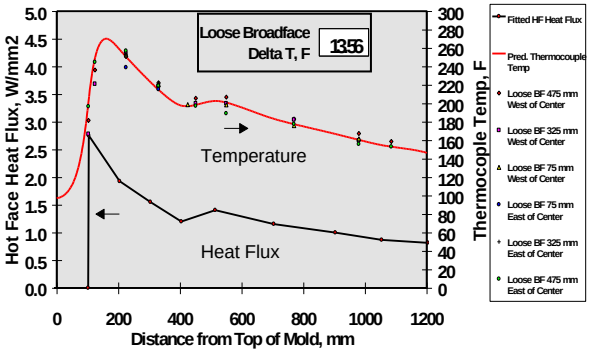

Figure 7 - Steady state temperature profile and calculated loose broadface heat flux for 409 stainless steel at 60 ipm.

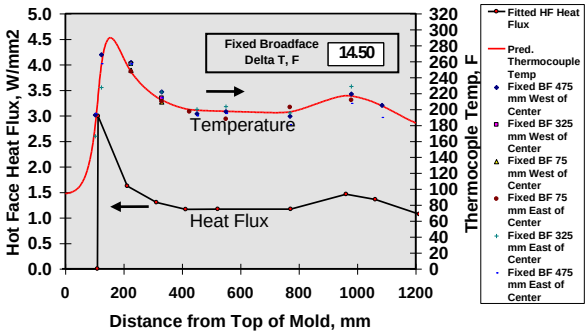

Figure 8 - Steady state temperature profile and calculated fixed broadface heat flux for 430 stainless steel at 58 ipm.

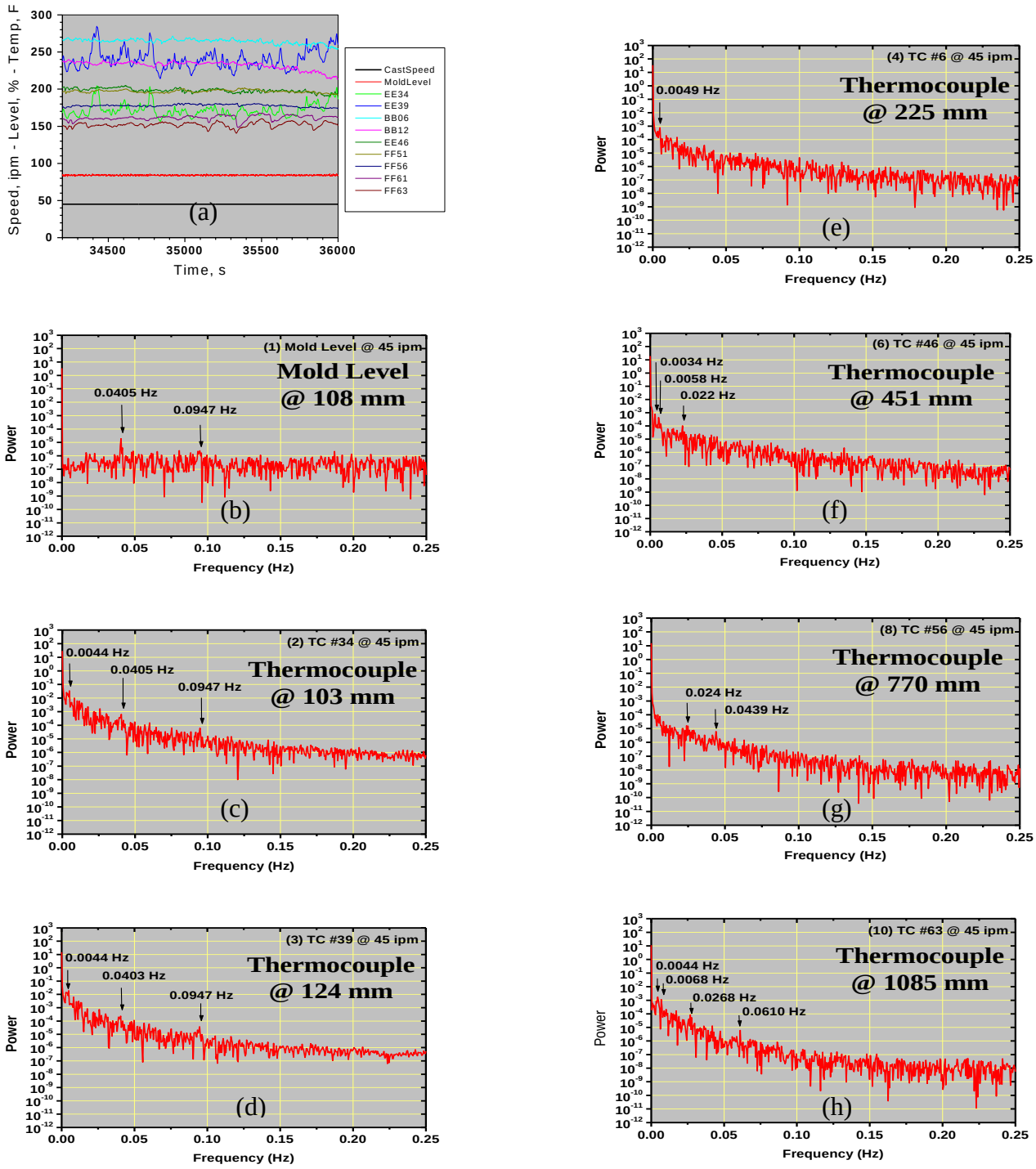

Figure 9 - Mold level and thermocouple signals at 475 mm West of mold centerline and various positions along the length of the mold for 409 cast at 45 ipm and corresponding Fourier power spectrum for each signal, (a) time domain signals used, (b) mold level in frequency domain, (c-h) mold temperatures in frequency domain.

meniscus, and that the mold temperature fluctuations tend to encompass a broad distribution of frequencies at the low end of the frequency spectrum with few discrete "signature" frequencies.

Transient Behavior

While steady state analysis of mold thermocouple data can provide important information about the thermal state of the mold during casting that is very helpful in the development of casting practices, the dynamic thermal behavior in the mold can only be inferred using steady state analysis, and much information on the dynamics is lost in the analysis. The use of more advanced tools, such as FFT analysis and cross spectral analysis[10] offer some improvement by providing means for interpreting cyclic and phase shifted thermal phenomena, however, the true dynamic behavior in the mold is often difficult to visualize when using these methods.

To facilitate the visualization of the transient thermal data collected with the instrumented mold at Mansfield, some simple software tools, like the one shown in **Figure 10**, were constructed to allow the spatial distribution of temperatures in the mold to be examined for each time step. These tools allow the data to be previewed easily using a scroll bar or played in animation using an indexing timer. The ability to scroll through large amounts of data and visually observe the transient mold thermal behavior in animation has been extremely useful in interpreting the thermal dynamics that take place within the mold, and has proved to be an invaluable tool in the development of casting practices in Mansfield.

Several examples of transient mold thermal behavior have been selected from the Mansfield mold thermal data, using these screening and visualization tools, for presentation in this

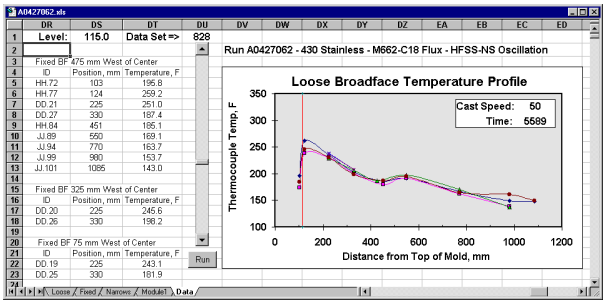

Figure 10 - Data analysis tool used for previewing and animating transient mold temperature data.

paper. Of course, only select "snapshots" for each example are presented here to attempt to convey the more important features observed in each animation, since displaying each frame of an animated sequence in print is not practical. The observations from each of these examples are presented in **Figures 11** through **17** and in the subsections that follow:

Transient Example 1

Short Duration Broadface Thermal Fluctuations in 1006 Carbon Steel at Steady State

The sequence of plots shown in **Figure 11** show the temperature profiles on the loose broadface for a 1006 carbon steel over a period of about 40 seconds. The thermal profile is remarkably stable and is the closest example of a true "steady state" condition that has been observed in our instrumented mold database. Despite this fact, some fluctuations in the vicinity of the meniscus are evident.

Transient Example 2

Short Duration Broadface Thermal Fluctuations in 409 Stainless Steel at Steady State

The sequence of plots shown in **Figure 12** show the temperature profiles on the loose broadface for a 409 stainless steel over a period of about 40 seconds. In contrast to the carbon steel example in **Figure 11**, the 409 example exhibits a somewhat more dynamic

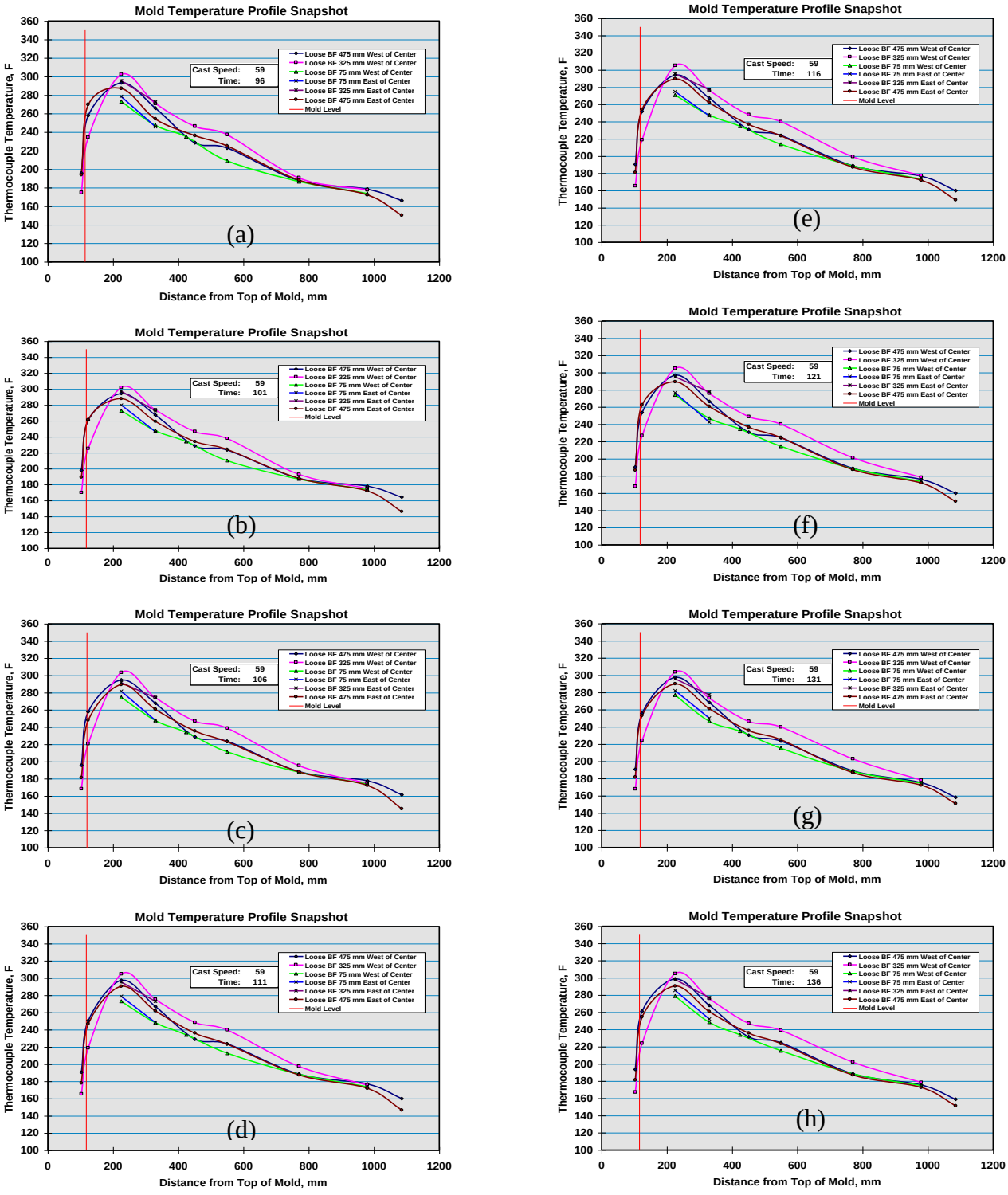

Figure 11 - ***Transient Example 1***

Sequence of mold temperature profile snapshots observed on the fixed broadface at 5 second intervals for low carbon steel (1006) cast at 59 ipm.

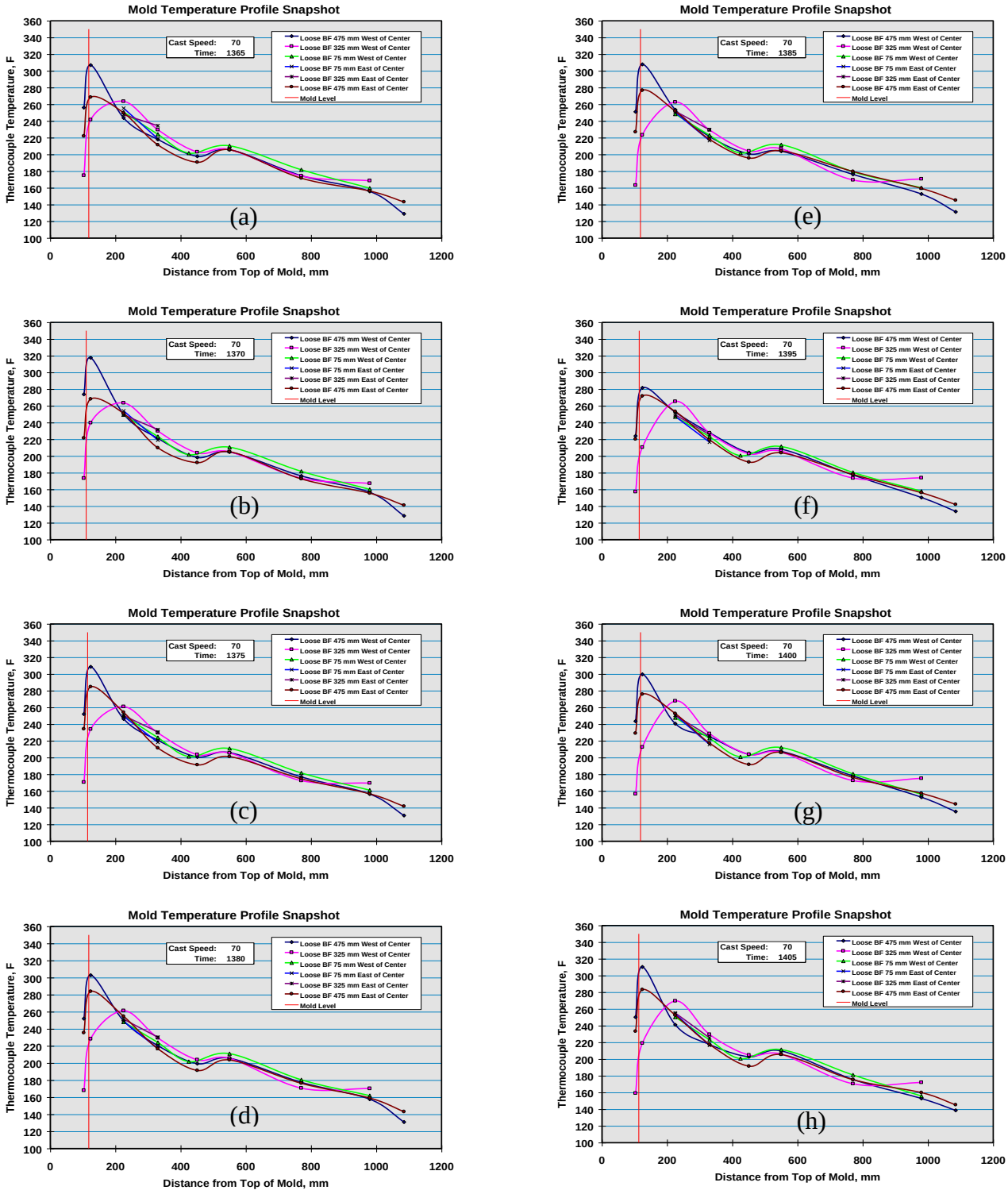

Figure 12 - ***Transient Example 2***

Sequence of mold temperature profile snapshots observed on the loose broadface at 5 second intervals for 409 stainless steel cast at 70 ipm.

thermal profile, particularly in the vicinity of the meniscus. Interestingly, the region of the thermal profile that displays the thermal "rebound" is relatively stable compared to the meniscus area. Occasional disruptions low in the mold that are difficult to capture in discrete frames are also evident in the animation.

Transient Example 3

Narrowface Thermal Fluctuations and Profile Changes in 409 Stainless During Speed Changes The sequence of plots shown in **Figure 13** show the temperature profiles on the two narrowfaces for a 409 stainless steel over a period of about 350 seconds during a casting speed change. In contrast to the broadfaces, the narrowface thermal profiles are much more dynamic on the Mansfield mold, even when the casting speed is constant. At the lower casting speeds, **Figure 13 (a)** through **(d)**, some thermal "rebound" is observed at the bottom of the mold. This "rebound" appears to diminish as casting speed increases, **Figure 13 (e)** through **(f)**.

Transient Example 4

Broadface Thermal Fluctuations and Profile Changes in 409 Stainless During Startup and Starter Powder Transition The sequence of plots shown in **Figure 14** show the temperature profiles on the loose broadface for a 409 stainless steel over a period of about 25 minutes following startup. The startup practice employs an exothermic starter flux at the start of the cast, followed by the application of the working mold flux at about 1 minute after startup. The interesting features to note in this sequence of profiles is that, while the starter flux is successful in establishing a stable thermal profile very quickly, **Figure 14 (b)**, the interaction of the starter flux with the working flux generates a transient destabilization of the thermal profile that takes almost 20 minutes to pass, **Figures 14 (c)** through **(f)**. After this transient period of mold flux interaction, the "steady state" profile is finally established for the working mold flux, **Figures 14 (g)** and **(h)**. It is interesting to note that the thermal profile disruption during the transition period is spatially very non-uniform. In **Figures 14 (c)**, for example, the disruption is localized in the west central portion of the mold.

Transient Example 5

Broadface Thermal Fluctuations in 1006 Carbon Steel Under Manual Mold Level Control The sequence of plots shown in **Figure 15** show the temperature profiles on the fixed broadface for a 1006 carbon steel during a manual mold level control training exercise just prior to cap-off. The example shows the effect of mold level fluctuations of up to 50 mm on the thermal profile along the length of the mold. Interestingly, the observed mold level disturbances do not appear to propagate deep into the mold, and instead appear to be localized to the region near the meniscus. This observation was also made earlier in the FFT analysis presented in **Figure 9**.

Transient Example 6

Broadface Thermal Fluctuations and Profile Changes in 409 Stainless With a Cracked SEN The sequence of plots shown in **Figure 16** show the temperature profiles on the loose broadface for a 409 stainless steel during a period when a hole developed in the SEN that was directed at the fixed broadface. The first anomaly observed in the thermal profile, **Figures 16 (b)** through **(d)**, is that the array of thermocouples closest to the SEN experience a significant increase in temperature along the entire length of the mold. At this stage, the other thermocouples are relatively unaffected by the problem. However, later in the cast, **Figures 16 (e)** and **(f)**, the thermal profile in the whole mold is disrupted and the thermal profile becomes dangerously erratic. The problem is finally overcome, **Figures 16 (g)** and **(h)**, by performing an SEN exchange, which restores the "steady state" profile.

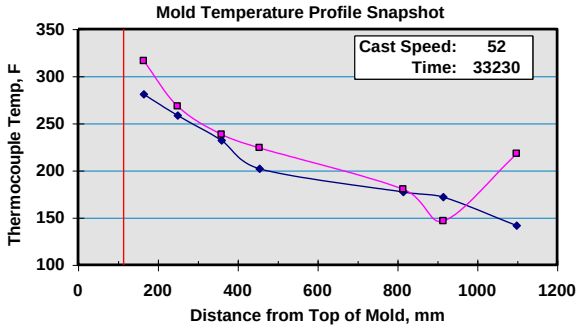

(a)

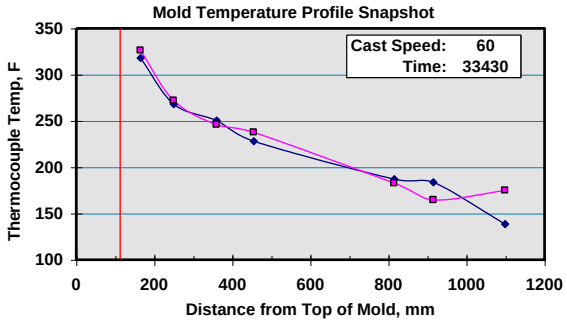

(e)

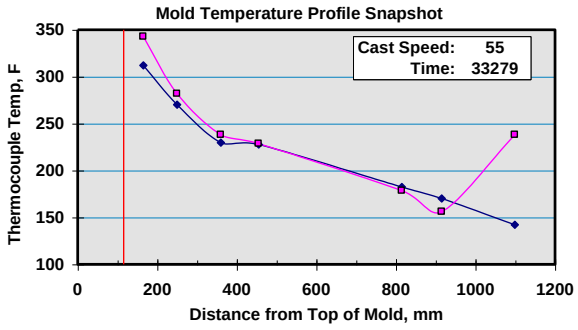

(b)

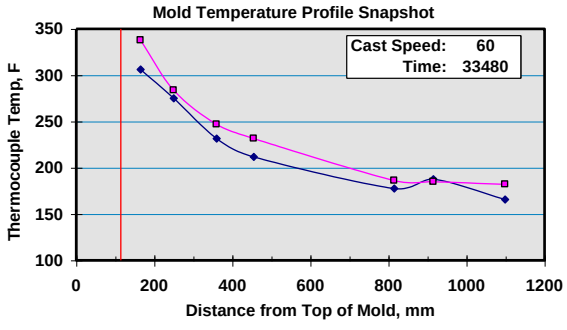

(f)

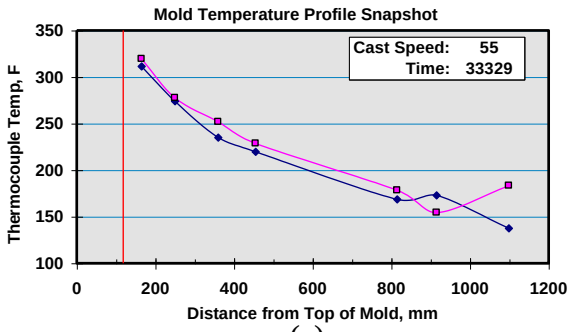

(c)

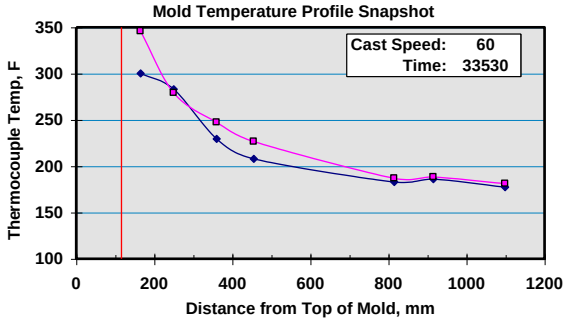

(g)

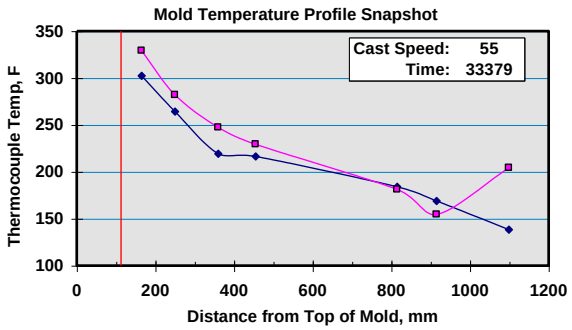

(d)

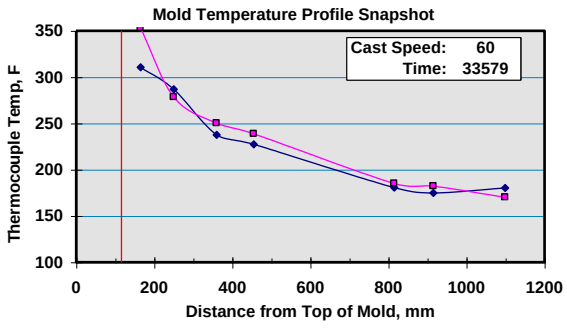

(h)

Figure 13 - ***Transient Example 3***

Sequence of mold temperature profile snapshots observed on the east and west mold narrowfaces at 50 second intervals for 409 stainless steel.

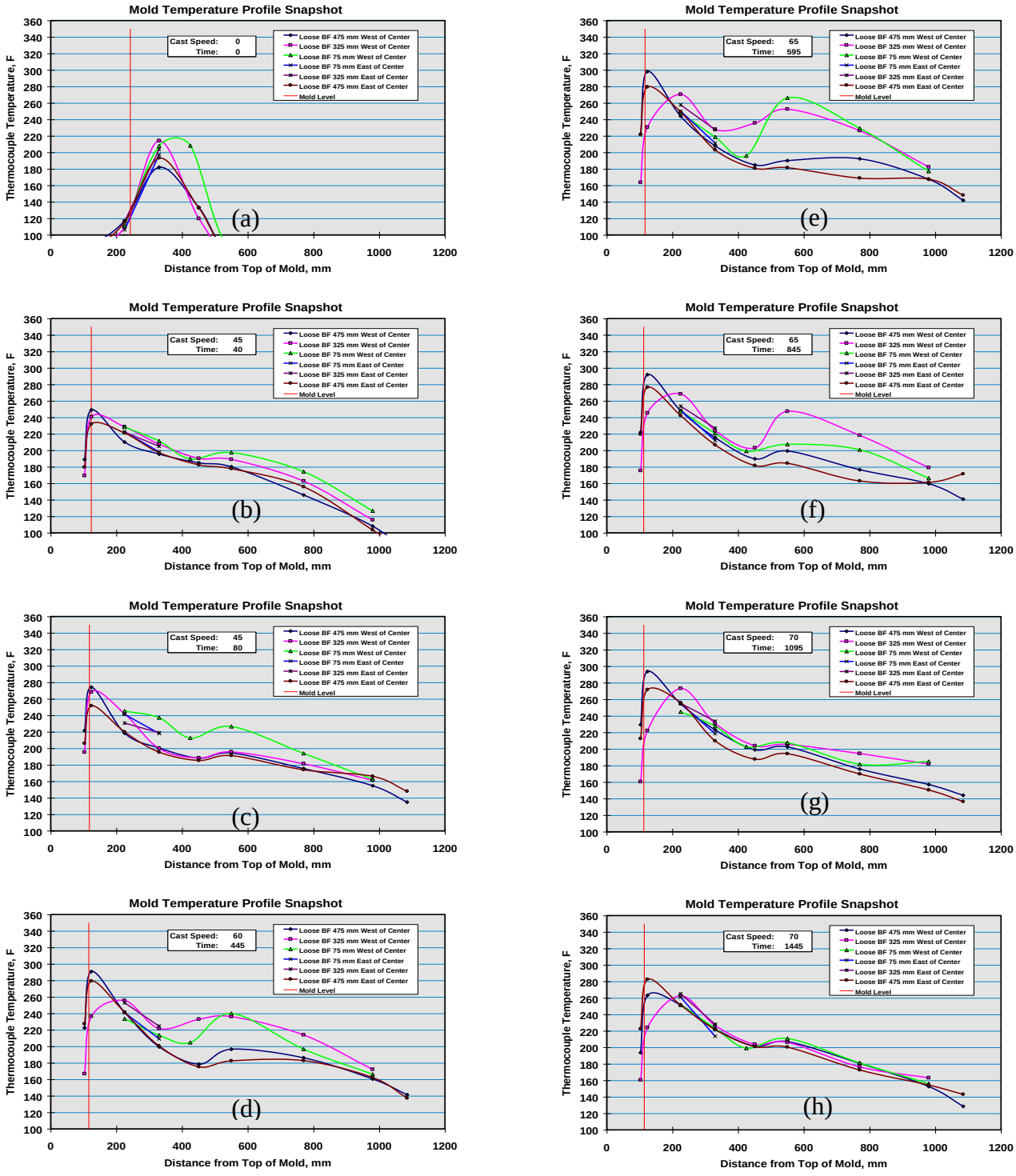

Figure 14 - *Transient Example 4*

Sequence of mold temperature profile snapshots observed on the loose broadface for a caster startup on 409 stainless, showing transition from starter flux to working flux.

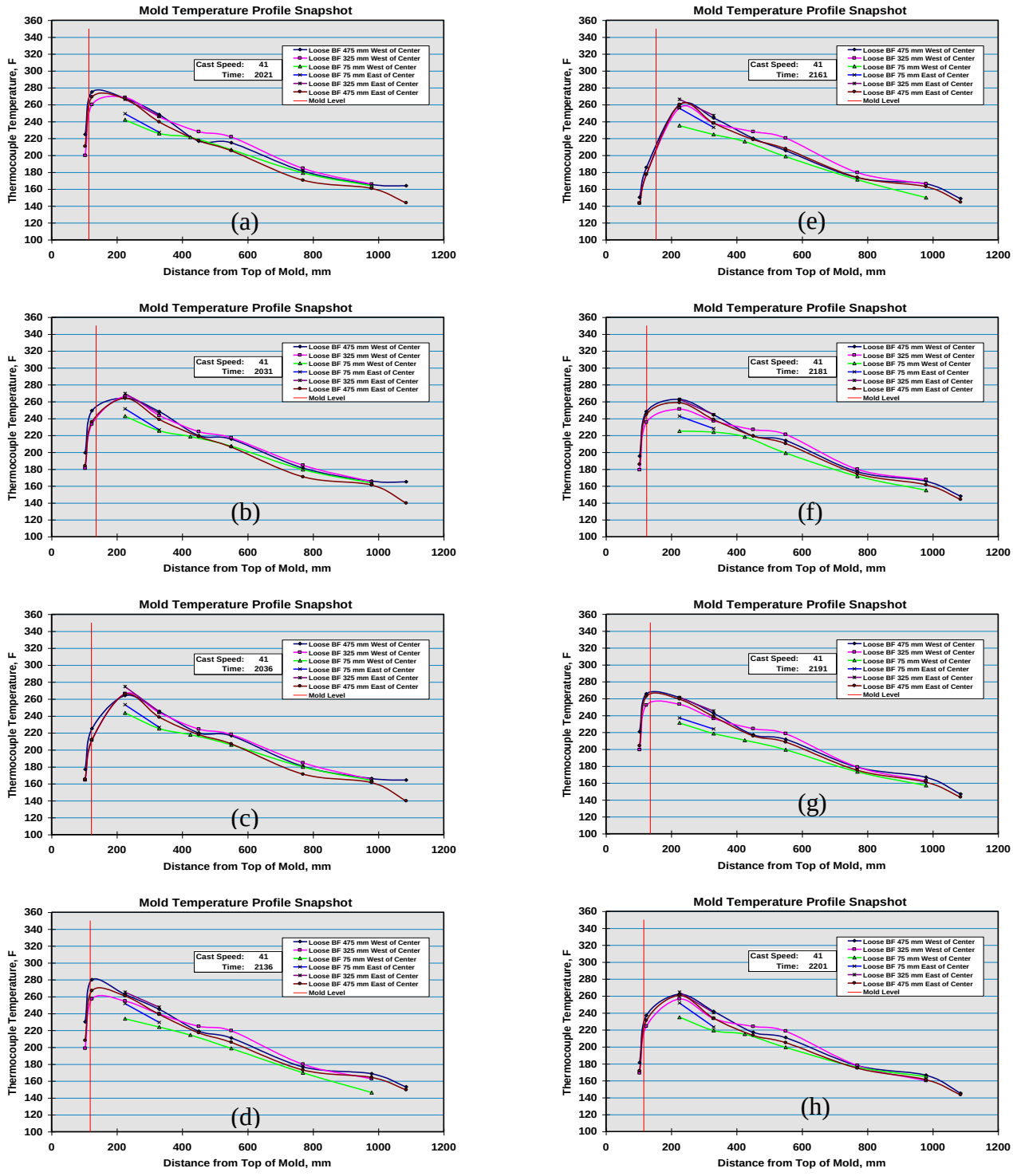

Figure 15 - *Transient Example 5*

Sequence of mold temperature profile snapshots observed on the loose broadface during manual mold level control training on 1006 carbon steel.

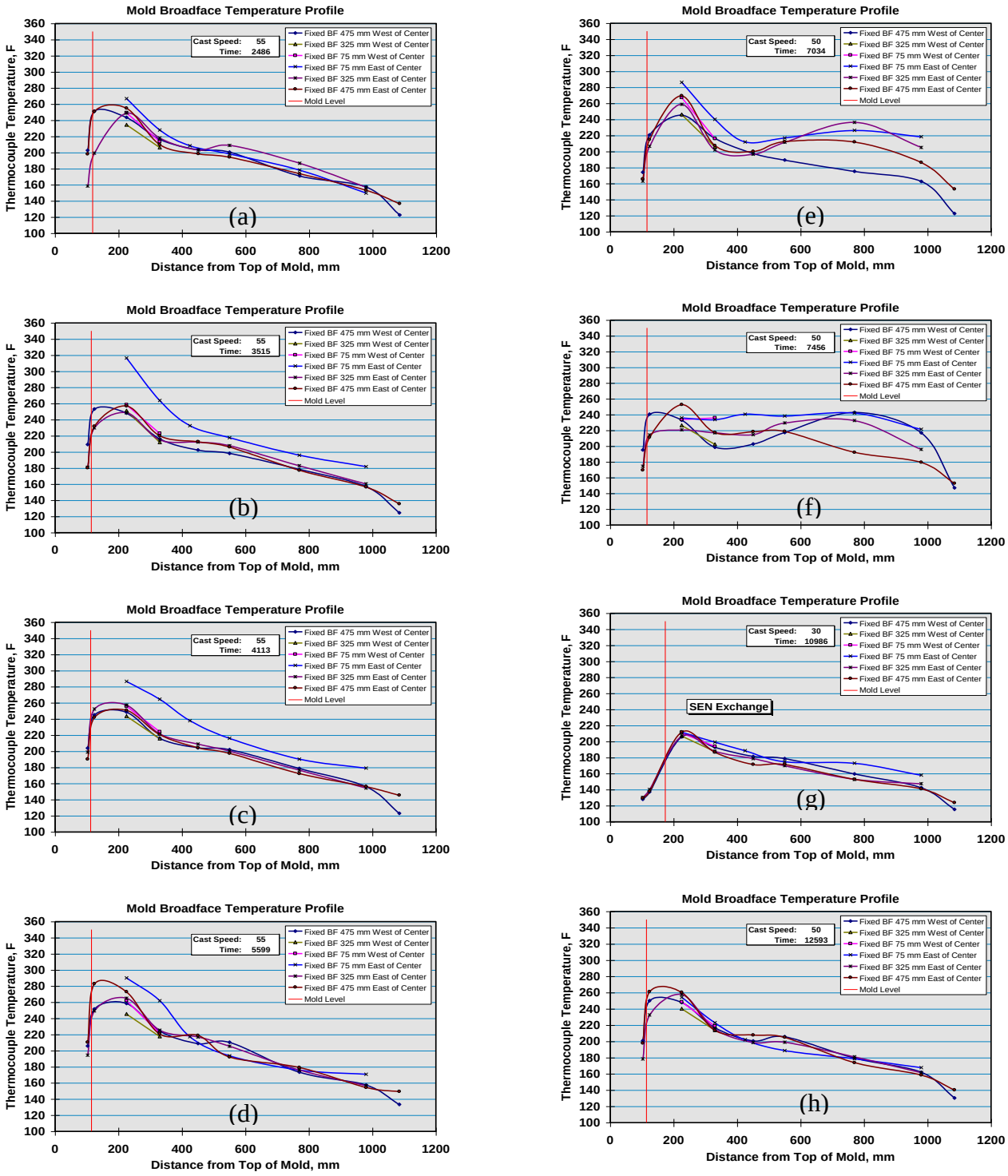

Figure 16 - ***Transient Example 6***

Sequence of mold temperature profile snapshots observed on a 409 stainless heat cast with a cracked SEN showing shell thinning, lubrication failure, and recovery through an SEN exchange to remove the cracked SEN.

Transient Example 7

Long Duration Broadface Thermal Profile Changes in 430 Stainless Steel The sequence of plots shown in **Figure 17** shows a plot of the mold water temperature rise for each mold face and some select temperature profiles on the fixed broadface for a 430 stainless steel corresponding to the times noted in **Figure 17 (a)**, spanning a time period of about 4.5 hours of cast time. In this example, the broadface mold water temperature rise gradually decreases with time over a period of hours, suggesting a continuous drop in heat removal on the broadfaces. The trend of decreasing heat removal appears to be broken when the casting speed is reduced for a short time, suggesting that this event "resets" the heat removal back to its original condition. In some cases, it appears that only one broadface is reset during a speed decrease.

The mold temperature profiles associated with this long term decrease in broadface heat removal**, Figures 17 (b) through (f)**, indicate that the drop in heat removal from the broadface is associated with a slowly changing temperature profile low in the mold, at about 500mm to 900mm below the top. Furthermore, unlike the gradual heat removal decrease, which occurs over several hours, the resetting of the thermal profile that is induced by a short reduction in cast speed occurs very rapidly and is sustained long after the event occurs.

DISCUSSION

The observations presented in the previous section cover a range of examples of steady state and transient mold thermal behaviors that have provided additional insight into the conditions that exist within the mold at Mansfield. In some cases, the causes of an observed behavior are relatively straightforward to interpret, whereas in other cases, the causes for the observed behavior can only be inferred based on the observations of the thermal behavior and other supporting evidence. Some interpretations of these observations are presented in this section.

Comparison of Steady State Profiles

The hot face heat flux and mold temperature profiles presented in **Figures 6** through **8** show that the 409 stainless and 430 stainless thermal profiles both exhibit a thermal "rebounding" condition that is not observed in the low carbon steel thermal profile, even though the peak heat removal at the meniscus is about the same for all three steel grades. The "rebound" in the 409 stainless example occurs at about one third of the way down the mold from the meniscus, whereas the thermal "rebound" for the 430 stainless example occurs at about two thirds of the way down the mold from the meniscus.

While the thermal profiles presented for these three grades do exhibit significantly different "rebound" behavior, the shape of the observed thermal profiles is not solely the result of differences in the three steel grades, but is also influenced by the mold powder and mold oscillation practice employed in the trial. An example of this can be seen by comparing the 430 stainless thermal profiles in **Figure 8** and **Figure 10**, which show thermal profiles for two different 430 stainless casting trials that were conducted using different mold powders and mold oscillation practices. The thermal profiles for these two cases differ significantly, particularly in their thermal rebound behavior.

The "rebound" observed in the thermal profiles for stainless is attributed to the difference in thermal shrinkage of these ferritic stainless grades and low carbon steel and to the differences in mold lubrication and mold oscillation strategies employed on each grade. The location and severity of the observed thermal re-

bound in these examples appears to be directly related to the rate that the hot face heat flux decreases from its peak value at the meniscus. The more rapidly the heat flux drops from its peak value, the lower in the mold and the more severe the thermal rebound is. This effect is believed to be attributed to differences in the solidifying shell's reaction to the peak heat removal near the meniscus and/or to the difference in flux film behavior in the gap between the mold and the shell below the meniscus. It is very likely that both factors play a significant role in this observed behavior.

Propagation of Mold Level Disturbances

Small disturbances in mold level have already been shown to influence thermal disturbances near the meniscus, **Figures 9(c)** and **(d)**, but not to effect the thermal fluctuations further down the length of the mold, **Figures 9(e)** through **(h)**. This example indicates that the "signature" disturbance frequencies observed at the meniscus at 0.4 Hz and 0.9 Hz in **Figure 9(a)** have dissipated at a distance of only 117 mm below the meniscus location. The transient thermal profiles in **Figure 15**, which show larger mold level disturbances associated with manual level control, also suggest that these larger disturbances do not propagate low into the mold.

In contrast to the observations made in this study, other investigators[8] have observed instances where mold level disturbances propagate down the entire length of the mold. The propagation of these disturbances has been attributed to the capture of the flux rim by a mold level disturbance and its withdrawal down the mold gap during casting[8]. The fact that this behavior has not been observed in this study, even with severe mold level fluctuations, suggests that the physical characteristics of the flux rim may influence its likelihood of capture during a large mold level disturbance. It is possible that the size of the flux rim and the strength of its adherence to the mold wall are important factors that influence the likelihood of flux rim entrapment and transport through the mold.

Starter Powder Transition

The thermal transition that is presented in **Figure 14** and **Example 4**, that is the result of the transition from a starter flux to a working mold flux during the first 20 minutes of startup, is one example of a long duration thermal transient that has been observed on the Mansfield caster. Experiments performed with varying amounts of starter flux have shown that the amount of starter flux does have an affect on the ability to form a stable thermal profile shortly after startup, **Figure 14 (b)**, but that it has little influence on the transition behavior with the working flux, **Figures 14 (c) through 14 (f)**. Observations of the startup behavior on other grades cast at Mansfield with different working mold fluxes but the same starter flux have shown that the duration of the thermal transition can vary greatly, with some flux combinations exhibiting almost no transition behavior and others exhibiting transition times of up to 30 minutes in duration.

The fact that the starter flux and the working flux both develop stable thermal profiles, **Figure 14 (b**) and **Figure 14 (h)**, but that the transition between the two exhibits a long period of poor thermal stability suggests that the thermal disturbance results from the interaction of the two fluxes in the mold gap. It is speculated that these slow transients are the result of the replacement of one solidified flux layer with another on the mold wall. The profiles in **Figure 14** suggest that this replacement occurs non-uniformly across the width of the broadface.

Other investigators[11] have observed that the mold powder transition within the mold gap occurs over a similar 20 minute time frame,

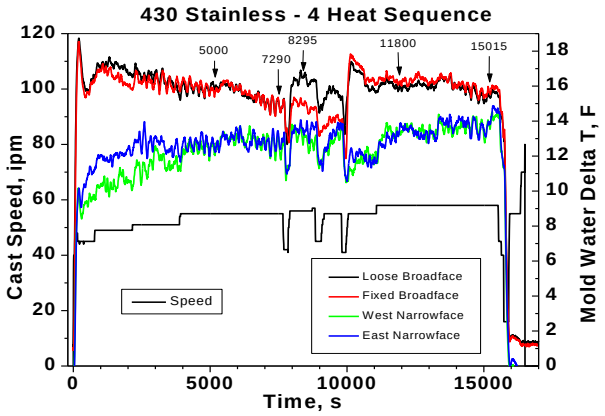

(a)

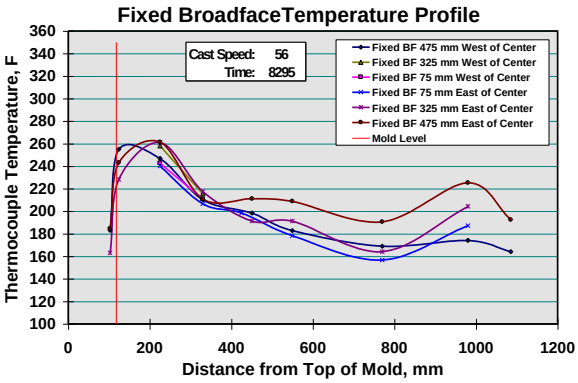

(d)

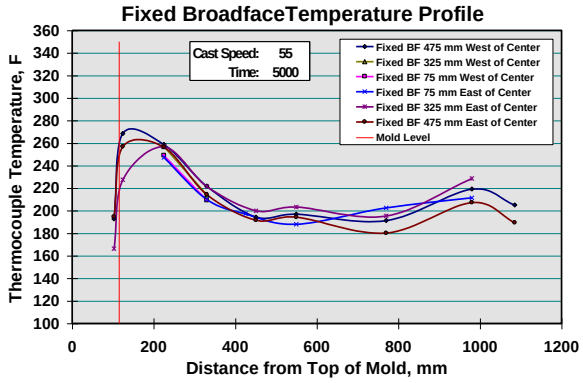

(b)

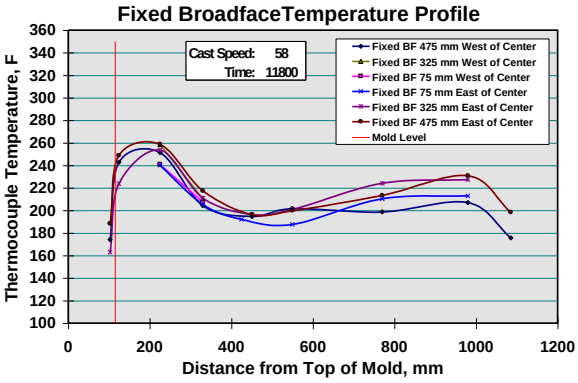

(e)

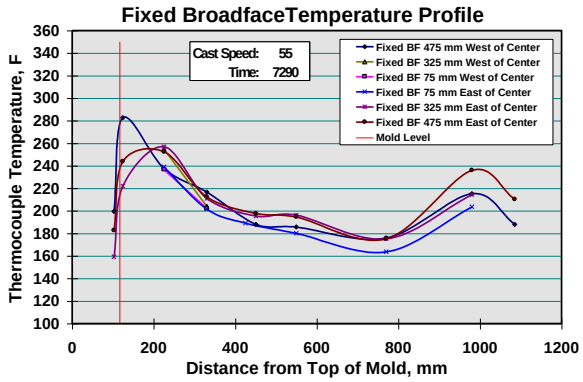

(c)

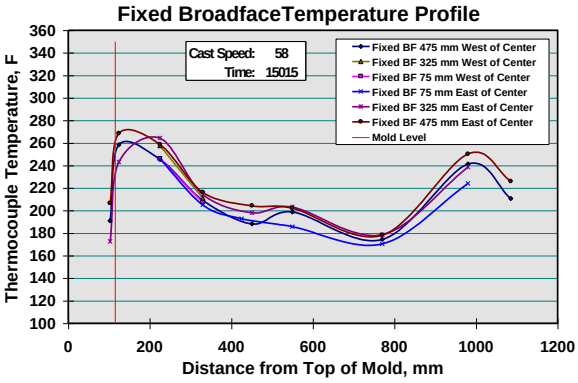

(f)

Figure 17 - Transient Example 7

Mold water temperatures and mold plate temperatures for 430 stainless: (a) Observed changes in mold water temperature rise in the mold during the cast, (b-f) broadface temperature profile snap-shots associated with observation times noted in (a).

but, that the powder transition occurs uniformly around the mold perimeter. The difference in the uniformity of the transition behavior between the previous study and this study may be related to the similarity of the properties of the two mold powders used in the prior investigation[11]. In the prior study, a tracer was used in an otherwise identical mold powder, whereas, in this study, the starter powder and the working mold powder have distinctly different properties. We believe that for certain combinations of starter and working fluxes, intermediate flux compositions that provide poor lubrication and heat transfer can be formed that destabilize the mold thermal profile during the transition.

Influence of SEN Condition

Two examples of the influence of a cracked SEN on mold thermal behavior can be seen in **Figure 16** and **Example 6**. The high temperatures on the single thermocouple array nearest to the crack, and the relative stability of the neighboring thermocouples in **Figures 16 (b)** and **16 (c)**, suggests that the hole in the SEN initiated below metal level and directed hot steel to the broadface at high velocity, where localized shell remelting occurred.

As time progressed, it appears that the crack expanded close enough to the meniscus area that air aspiration began to occur. This air aspiration is believed to have loaded the mold flux with oxidized components that gradually affected the flux's ability to lubricate the mold and provide stable heat transfer. At this point, **Figures 16 (e)** and **16 (f)**, the thermal stability of the whole mold is affected because the liquid flux that feeds the gap has become contaminated with reoxidation products. The localized remelting of the shell also appears to have diminished at this time, suggesting that the hole in the SEN has become enlarged, the impingement velocity on the broadface has decreased, and less localized melting of the shell has occurred. The replacement of the SEN ultimately returned the mold to a stable thermal condition with uniform temperatures.

The crack in the SEN was actually not observed until after the SEN was removed and examined. In fact, during the trial, the operators suspected that a problem existed in the mold only after the breakout predetection thermocouples began to behave erratically. No one was aware of how close we actually came to a breakout in this campaign until after the SEN change, when the hole in the SEN was discovered and the thermal data was examined.

Long Duration Transients on 430 Stainless

The transient thermal behavior presented in **Figure 17** and in **Example 7** for a 430 stainless steel development trial shows the longest duration transient thermal behavior that we have seen to date in our investigations at Mansfield. In this example, the mold heat removal and thermal profiles are still continuing to change two hours after the start of the cast. What is, perhaps, more interesting is that the whole downward trend in broadface heat removal is reset by a modest reduction in casting speed of relatively short duration. The mold heat removal and thermal profiles quickly return to their initial state after the speed change and then gradually evolve to their previous long term state over a period of hours.

Interestingly, in our initial development of the casting practices for 430 stainless, we experienced conditions shortly after we started to sequence cast 430 stainless with this practice where, by chance, no reductions in cast speed occurred for several heats. The heat removal on these sequences continued to decrease until either excessive slab bulging or a breakout occurred. While the instrumented mold was

not available for these trials, the mold heat removal data indicates that the same type of long term drop in broadface heat removal that is observed in **Figure 17 (a)** also occurred in these cases, but without the resetting associated with a speed reduction.

The thermal profile changes that occurred during this long duration thermal transient indicate that the drop in broadface heat removal with time results from a gradual decrease in heat transfer low in the mold. This can be seen more clearly in the heat flux profiles presented in **Figure 18**, which were calculated from the thermal profiles presented in **Figures 17 (b)** and **17 (c)**. The plot suggests that the slow drop in heat removal occurs in the region between 500 mm and 900 mm below the top of the mold.

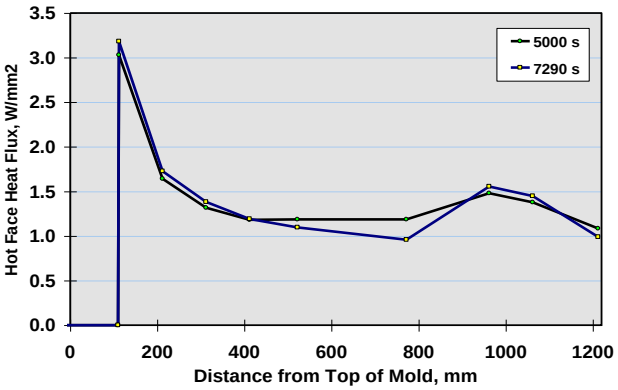

Figure 18 - Calculated fixed broadface heat flux profiles showing area in mold responsible for long term transient heat removal decrease in 430 stainless.

The dependence of the mold heat removal on casting speed observed in **Example 7** is similar to the *hysteresis* in mold temperature vs. speed reported by Ogibayashi, et.al.[11], but differs in two ways. First, the *hysteresis* reported previously did not exhibit a slow decrease in heat removal at constant speed. Second, the thermal *hysteresis* observed in the prior examination was reported to occur at all locations within the mold, whereas, this investigation has found that the thermal *hysteresis* only occurs in the lower part of the mold.

To explain the transient thermal behavior observed in this examination, the mechanism outlined in **Figure 19** is proposed. Under the conditions of the casting trial in **Example 7**, a strongly adhering layer of crystalline mold flux develops on the mold wall. As time progresses, the layer continues to build low in the mold. Where the kinetics of crystal growth are sluggish, this buildup occurs very slowly. If left at steady casting speeds, this layer continues to grow until the steel shell growth is sufficiently retarded that excessive bulging or a breakout occurs. With a moderate speed reduction, however, the change in thermal conditions in the gap and/or the increase in friction low in the mold causes part of the crystalline film to fracture and be withdrawn with the slab. When the normal casting speed is resumed, a new crystalline layer is reformed and the whole process repeats itself.

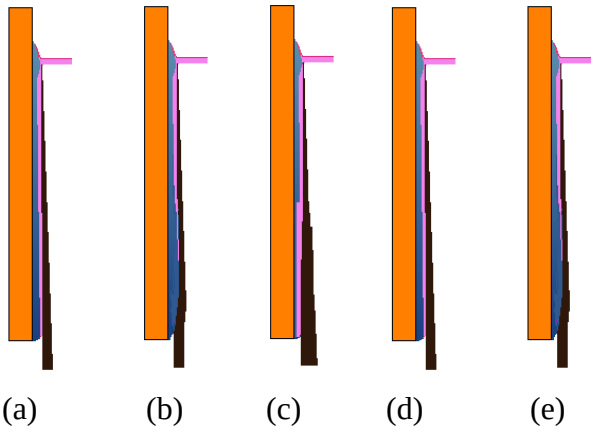

Figure 19 - Proposed mechanism for reversible long term heat removal decrease on 430 stainless, (a) developed crystalline layer, (b) excessive layer buildup low in mold, (c) shear-off of lower layer at lower speed, (d-e) repeat of (a) and (b).

Indirect evidence for the presence of an adhering and fracturing mold powder film on the mold wall can be found in previous investigations. Ozgu, et.al.[6], observed "sawtooth-like" thermal fluctuations low in the mold that they

attributed to periodic fracturing of the flux film. Similar patterns can be observed on the lower thermocouple traces in the 409 example shown in **Figure 9 (a)**. Spectral analysis, **Figure 9 (h)**, suggests that the rate of fracture occurs over a wide range of frequencies, with a modest peak on a 3.8 minute cycle. This mean fracture cycle time is in the same frequency range reported by Ozgu, et.al.[6]

In addition, Ogiayashi, et. al.[11] have shown that a portion of the flux film within the mold gap must travel at a much lower speed than the strand to account for the long transients observed in their tracer studies, suggesting that the solid flux film is retained within the mold gap for an extended period of time.

Some direct evidence for the proposed mold powder sheeting mechanism is also shown in **Figure 20**. This micrograph shows the cross section of a mold powder film that was removed from the mold wall at cap-off at about 300 mm from the top of the mold. The solid layer against the mold side of the sample is interpreted to be the stationary crystalline flux layer, and the sheets of crystalline flux within the glassy region are interpreted to be sheets of crystalline material that have been sheared from the stationary layer and carried down the mold gap in the liquid layer. A number of similar examples of shearing behavior have been observed in flux films taken from the mold wall during cap-off at Mansfield.

The reason that the long term crystalline layer buildup occurs low in the mold in the 430 example presented in **Figure 17** is not entirely clear, but may be related to the nature of the crystallization behavior of the mold powder employed in **Example 7**. It is generally well known that the crystallization behavior of mold powders can be characterized using time-temperature-transformation (TTT) diagrams that describe the crystallization phenomena for mold fluxes over a wide range of cooling conditions[12], as shown in **Figure 21**. In the upper part of the TTT curve, crystallization is inhibited by the small thermal driving force for nucleation, i.e., low undercooling. In the lower part of the TTT curve, however, crystallization is inhibited by low temperatures that make crystal growth sluggish. The slow crystalline layer growth observed in the lower part of the mold in **Figure 17** is believed to coincide with the lower portion of TTT curve for the mold flux employed in **Example 7**.

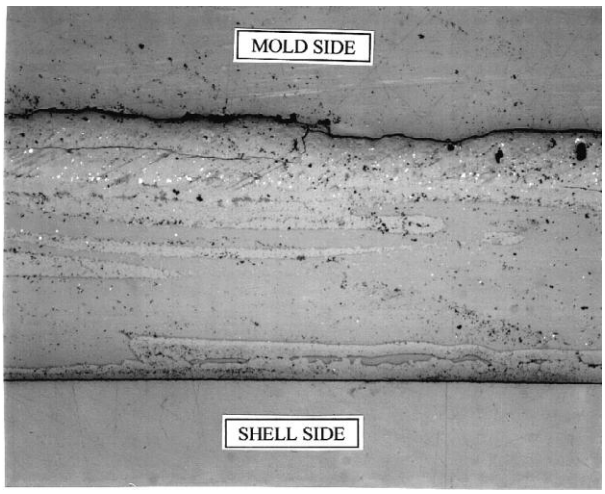

Figure 20 - Polished cross section of flux film taken from mold wall at capoff showing evidence of sheared crystalline layers in the film.

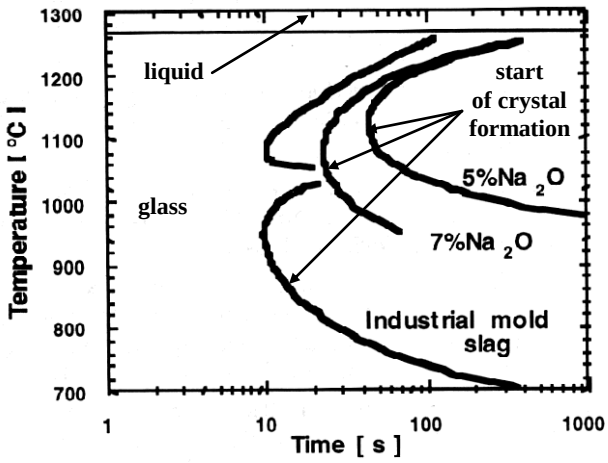

Figure 21 - TTT Diagram for simulated and industrial mold fluxes after Kashiwaya, et.al.[12]

High in the mold, where the crystal growth kinetics are favorable, a steady thermal profile is established rapidly and sluggish crystal growth is not observed because nucleation sites already exist on the mold wall. However, the sluggish crystallization kinetics in the region of the TTT curve which corresponds to the lower part of the mold, combined with a crystalline layer that resists shearing until a process change such as a speed change is encountered may explain the transient thermal behavior that is observed in the 430 example presented in **Figure 17**.

SUMMARY

The methods of analysis presented in this paper have allowed thermal data collected using an instrumented mold on the Mansfield caster to be examined under steady state and transient conditions. A comparison of the steady state thermal profiles obtained for 1006 carbon steel and for 409 and 430 stainless steel has revealed that the ferritic stainless steels exhibit a thermal rebound condition on the mold broadface that is not observed in the low carbon steel. This rebound behavior is shown to be influenced by changes in mold lubrication and mold oscillation practice.

In addition, the magnitude of thermal fluctuations and the severity of the broadface thermal rebound observed for these examples increased in the following order: 1006 < 409 < 430, even though the peak heat removal for each was about the same. Also, the thermal fluctuations on the mold narrowfaces were observed to be larger in magnitude than those observed on the broadfaces.

The transient thermal effects from an SEN failure were also presented. In addition to localized shell melting which resulted from hot steel impingement on the shell, the influence of air aspiration on mold lubrication was also observed in the mold thermal data. The breakdown of mold lubrication was attributed to the buildup of deoxidation products in the mold powder after air aspiration through the hole began to occur.

Transient thermal behaviors that range from seconds to hours in duration have also been presented. The shortest duration thermal fluctuations were observed near the meniscus. These fluctuations were found to contain the same "signature" frequencies as those observed in the mold level disturbances, which had a cycle time of 10 to 30 seconds. At only a modest distance from the meniscus, the thermal fluctuations associated with mold level disturbances disappeared, and only a broad distribution of low frequency disturbances remained. These thermal fluctuations, which exhibited cycle times that varied from 30 seconds to 5 minutes in duration, were postulated to result from the periodic sheeting of crystalline mold flux from the mold wall.

Two conditions under which long time duration thermal transients were observed were also presented. The first example, which involved the transition from a starter flux to a working mold flux at startup on a 409, exhibited a period of transient thermal instability of 20 minutes, despite the fact that a steady thermal profile was established for both fluxes before and after the transition period. The second example, which involved a steady but gradual decrease in broadface heat removal with time on a 430, occurred over a period of hours, but was reset almost instantaneously with a small speed change. The source of both of these long duration thermal transients is proposed to result from the behavior of the stationary crystalline flux film within the mold gap. Evidence for mechanisms involving sluggish crystal growth and rapid crystalline layer sheeting is presented.

ACKNOWLEDGEMNTS

The author would like to thank Josef Watsinger and Andy Flick of VAI for their support of the joint development project work that made this study with the instrumented mold at Mansfield possible. The special efforts of Jim Unglesby, and Brian Grant at Armco's Technology Center and the "Caster ET's" at Mansfield, that contributed to the installation of an operating mold with 106 thermocouples that all worked on the first try, are greatly appreciated. The efforts of all of the individuals at Armco's Technology Center, Armco's Mansfield Operations, VAI, and VAST who contributed to the work presented in this paper are also gratefully acknowledged.

REFERENCES

1 "Casting Technologies Supporting the Development of Direct Hot Charged Carbon and Stainless Steel Production at Armco's Mansfield Operations", R. J. O'Malley: *Proc., 39th Mechanical Working and Steel Processing Conf*., ISS, Indianapolis, IN, pp. 849-860, 19-22 October, 1997.

2 "Measurement of Temperature, Solidification, and Microstructure in a Continuous Cast Thin Slab", B. G. Thomas, R. J. O'Malley, and D. Stone, *Proc. Modeling of Casting, Welding & Advanced Solidification Processes VIII*, San Diego, CA, pp. 1185-1199, June 7-12, 1998.

3 "An Experimental Instrumented Mold for Heat Transfer and Operating Conditions Study", R. Sobolewski, S. Sander, J. Kuczma, and A. Rumler, *ISS Steelmaking Conference Proc.*, Vol. 74, pp. 275-280, 1991.

4 "Heat Transfer in Continuous Casting when Using Different Mold Powders", H. Abratis, F. Hofer, M. Junemann, J. Sandemann, H. Stoffel, *Stahl und Eisen*, Vol. 116, No. 9, pp. 73-78 & 155, 1996.

5 "Improvement of Surface Quality of Continuously Cast Slab", Y. Miyashito, M. Suzuki, K. Taguchi, S. Uchida, H. Sato, M. Yamamura, *Nippon Kokan Tech. Rpt*., Overseas No. 36, pp. 55-64, 1982.

6 "Thermal Analysis of the Burns Harbor No. 2 Slab Caster Mold", M. Ozgu, B. Kocatulum, *I&SM*, pp. 77-84, May, 1994.

7 "Thermal Monitoring of the CC Mold for the Control of Solidification and Slab Surface Quality", A. Delhalle, J. Genneson, G. Krausener, J. Lanaut, M. Larrecq, M. Niederlander, *Proc. ECSC Workshop on Steelmaking, Steel Cleanliness, and Mold Thermal Monitoring*, European Comm. Luxemburg, pp. 197-201, Nov. 24-25, 1993.

8 "Investigation of Strand Surface Defects Using Mold Instrumentation and Modeling", M. Jenkins, B. Thomas, W. Chen, R. Mahapatra, *ISS Steelmaking Conference Proc.*, Vol. 77, pp. 51-71, April, 1991.

9 "Spread Sheet Model of Continuous Casting", B. Thomas and B. Ho, *Trans. ASME*, Vol. 118, pp.37-44, Feb., 1996.

10 "Analysis of Shell Thickness Irregularity in Continuously Cast Middle Carbon Steel Slabs Using Mold Thermocouple Data", J. Suni, H. Henein, *ISS Steelmaking Conference Proc.*, Vol. 79, pp. 331-335, 1993.

11. "Mold Powder Technology for Continuous Casting of Low-Carbon Aluminum-Killed Steel", S. Ogibayashi, T. Mukai, Y. Mimura, Y. Nagano, K. Yamaguchi, T. Takahashi, K. Koyama, T. Nakano, *Nippon Steel Technical Report*, No. 34, pp. 1-10, July 1987.

12. "Crystallization Behavior of Mold Slags", Y. Kashiwaya, C. Cicutti, A. Cramb, , *ISS Steelmaking Conference Proc.*, Vol. 81, pp. 185-191, 1998.